

Size dependence of intrinsic spin transfer switching current density in elliptical spin valves

R. Heindl,^{1,a)} S. E. Russek,¹ T. J. Silva,¹ W. H. Rippard,¹ J. A. Katine,² and M. J. Carey²

¹National Institute of Standards and Technology Boulder, Colorado 80305, USA

²Hitachi Global Storage Technologies, San Jose Research Center San Jose, California 95135, USA

(Received 15 April 2008; accepted 12 June 2008; published online 2 July 2008)

We studied current-induced magnetization reversal in elliptical spin valves with CoFeB free layers. The data obtained from high-speed pulsed switching experiments showed that the intrinsic switching current densities were size dependent and 50%–100% higher than predicted by a single-domain model. Micromagnetic simulations reveal a complex behavior of magnetization switching in which end-mode oscillations are important, and indicate that the switching current density depends on the device dimensions. Experimental values for the intrinsic switching current density agree with those predicted by micromagnetic simulations. © 2008 American Institute of Physics. [DOI: 10.1063/1.2953980]

Recently, there has been considerable interest in current-induced magnetization switching of nanoscale magnetic devices using spin-polarized currents^{1–3} for applications in the next generation of magnetoresistive random access memory devices. For applications in nonvolatile memories, fast switching (periods less than 1 ns) with low current pulses is of particular interest.⁴ In order to understand complicated magnetization behaviors in nanoelements that involve multi-domain configurations, domain oscillations, and domain wall movements (all of which are not included in the single-domain model), micromagnetic simulations have been used by several research groups.^{5–7}

We report in this paper our study of dc-sputtered current-perpendicular-to-plane giant-magnetoresistive spin-valve nanopillars consisting of the following structure: bottom electrode (5 nm Ta|30 nm Cu|3 nm Ta|30 nm Cu|5 nm Ta|2 nm Ru), synthetic antiferromagnet (SAF) layer pinned to IrMn (7 nm IrMn|3 nm Co₅₀Fe₅₀|0.8 nm Ru|3 nm Co₅₀Fe₅₀), metallic spacer (4 nm Cu), free layer (3 nm Co₆₀Fe₂₀B₂₀), and top electrode (20 nm Cu|5 nm Ru|2.5 nm Ta). Electron-beam lithography and subsequent ion milling were used to pattern the thin-film structure into ellipses. Devices with dimensions from 104 × 40 nm² to 200 × 100 nm² were fabricated and measured. We present data from two sets of devices with different sizes: 104 × 40 nm² (aspect ratio AR=2.6) and 177 × 60 nm² (AR=2.95). All devices were made on the same chip in the same process.

The experimental setup is similar to that described in Ref. 8, consisting of a nanopillar device mounted in a coplanar waveguide (CPW) structure with signal conductor on the top and the ground conductor on the bottom of the nanopillar. The CPW structure is contacted with high bandwidth probes, and a current pulse is sent to the device. The device is initially set in the high-resistance antiparallel (AP) state, and a current pulse is then applied to the device in order to attempt to switch it into the parallel (P) state. Subsequent to the pulse, the resistance of the device is measured through the inductive (low frequency) leg of the bias-tee by use of a lock-in amplifier to determine whether switching occurred or not, i.e., whether the device is in the low (P) or the high

resistance (AP) state. This process was repeated 100 times at each current amplitude and pulse duration to determine the switching probability. During the measurements, a small in-plane magnetic field was applied to counterbalance the dipole field coupling with the fixed layer. In addition, a dc bias current was applied to the device to make AP-P and P-AP switching symmetric. About ten devices of each size were tested, and measurements showed that for nominally identical devices, the variations in the device resistance, magnetoresistance, and low frequency switching fields and currents were small, typically less than 5%. In addition, the difference in the resistance × area (RA) products for devices of different sizes was also less than 5%.

The data of Fig. 1 show the switching probability P_s as a function of the pulse current duration t_p at various current densities for two representative devices. The intrinsic switching current density Jc_0 is the current density required to switch a device for arbitrarily long pulse duration in the absence of thermal fluctuations (at $T=0$ K). Similar to the procedure in Ref. 8, Jc_0 was calculated from the data in Fig. 1 by fitting the pulse duration needed for 50% switching probability versus pulse current magnitude, followed by fitting t_{50} versus I to a function $t_{50}=a(I-Ic_0)^{-b}$. Here, however, the

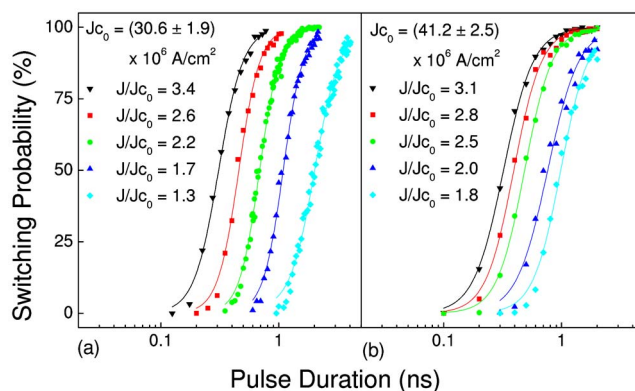


FIG. 1. (Color online) Switching probability distribution as a function of pulse duration for various pulse amplitudes (data taken at $T=300$ K). Jc_0 is the extrapolated intrinsic switching current density for long pulse durations at $T=0$ K. Solid lines are the fits to the data. (a) 104 × 40 nm² ellipse, (b) 177 × 60 nm² ellipse.

^{a)}Electronic mail: heindl@nist.gov.

switching probability curves were fit to a sigmoidal Hill function [$P_s = 100 \times (t_p^n / (t_p^n + t_{50}^n))$], rather than to Fermi functions, which gives a better fit to the data. From these measurements Jc_0 for the two devices is different: $(30.6 \pm 1.9) \times 10^6$ A/cm² for the 104×40 nm² ellipse and $(41.2 \pm 2.5) \times 10^6$ A/cm² for the 177×60 nm² ellipse. This cannot be explained with a single-domain model used to predict the intrinsic current density,² which gives values of about 20×10^6 A/cm² for the two devices, using:⁹

$$Jc_0 = 3.77 \times 10^9 \times \frac{\alpha M_s d (H_k + H_{\text{free}} + M_s/2)}{\nu P} \left(\frac{1}{Am} \right) \quad (1)$$

with $\nu = 8\sqrt{P[(3 \pm 1)(1+P)^3 - 16P^{3/2}]}^{-1}$, where α , M_s , d , and P are the damping constant, saturation magnetization, free layer thickness, and spin polarization of electrodes, respectively. H_k is the in-plane anisotropy (mainly shape) and H_{free} is the total magnetic field at the free layer. We use the measured values for CoFeB of $M_s = 1150$ kA/m, $\alpha = 0.012$, $P = 0.4$, $H_{\text{free}} = 0$. The shape anisotropies (H_k) were calculated to be 39 and 25 kA/m for the 104×40 nm² and 177×60 nm² ellipses, respectively, and are too small compared to M_s to appreciably alter the values of Jc_0 calculated using Eq. (1). As can be seen from Eq. (1), the single-domain model predicts a constant current density independent of the device size, assuming all other values are equal. For completeness, we also used Landau–Lifshitz–Gilbert macrospin simulations (that include the spin-torque effect) to estimate the intrinsic switching current at $T = 0$ K for the $104 \times 40 \times 3$ nm³ and $176 \times 60 \times 3$ nm³ rectangular devices (for simplicity we chose rectangular devices and the calculated shape anisotropies for the rectangles were similar to those of the ellipses). Using the same parameters as above, the intrinsic current density is about 20×10^6 A/cm² for both device structures, which is the same as the value obtained using Eq. (1).

In order to understand the discrepancy between the experimental values of Jc_0 for the two devices and those calculated by the single-domain model, as well as the variation in Jc_0 depending on the device size and geometry, we performed a set of micromagnetic simulations using OOMMF with the three-dimensional solver modified to include spin torque term,¹⁰ $\tau_{\text{st}} = \gamma \beta \varepsilon [\vec{m} \times (\vec{m} \times \vec{m}_p)]$, where γ is the gyromagnetic ratio, \vec{m} is the normalized free layer moment, \vec{m}_p is the normalized fixed layer moment, $\beta = (\hbar \mu_0 e) / (I \Omega M_s)$, Ω is volume, and $\varepsilon = P/2$. A fieldlike term was not included and a constant efficiency ε was used.¹¹ Only the free-layer dynamics were calculated in the simulations. The fixed layer was assumed to have a constant magnetization direction and no magnetostatic interactions between the fixed and the free layer were included. The current I was assumed to be uniformly injected through the device, and the current-generated fields (Oersted fields) were calculated and included in the simulation. The exchange stiffness was taken to be $A = 20 \times 10^{-12}$ J/m, and all other parameters were as indicated above. The currents were applied instantaneously, as opposed to the experimental pulses, which had a rise time of 45 ps.

In order to determine the intrinsic switching current density, we simulated switching at $T = 0$ K at various applied currents for a number of elliptical devices with different areas (3 nm thickness) and aspect ratios. Long axes were varied from 30 to 280 nm, and short axes were varied from

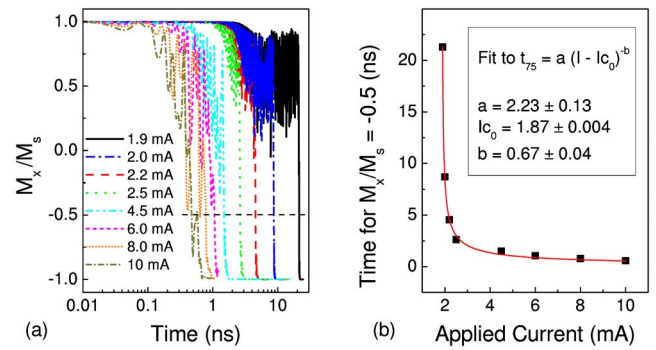


FIG. 2. (Color online) Micromagnetic simulation of magnetization switching for the case of a 160×40 nm² ellipse. (a) Time evolution of the average x -component of the magnetization at various applied currents. (b) Fitting procedure to determine the intrinsic switching current.

10 to 90 nm, while the aspect ratios used were between 1 and 6. The intrinsic currents were determined in a way similar to that used to extract Jc_0 from the experimental data. The time needed for the magnetization to switch from +1 to -0.5 (75%) was plotted versus the applied current, and from the fits to these plots we were able to extract the values of the intrinsic switching current densities. Figure 2 shows representative plots for the simulated magnetization switching, the switching time t_{75} versus pulse current amplitude, along with the fit used to find the values of the intrinsic switching current. Before switching occurs, one can clearly see oscillations in the magnetization, which will be discussed further below.

Figure 3 shows the distribution of the values of Jc_0 as a function of device area for different device aspect ratios. There is a roughly linear increase in Jc_0 with area, but no clear dependence on aspect ratio. In all cases of smaller devices, the values of Jc_0 are comparable to the values obtained from the single-domain model. For the two devices used in experiments, the simulations give values of $Jc_0 = 30.5 \times 10^6$ A/cm² for the 104×40 nm² ellipse, and $Jc_0 = 33.3 \times 10^6$ A/cm² for the 176×60 nm² ellipse. These values are close to the experimental values and also show the difference in Jc_0 between the two devices. Further differences between the experimental and simulated values could be attributed to nonideal shapes and sizes of the elliptical devices used in the experiments.

Next, we simulated the time-dependent magnetization for pulsed current densities very close to the intrinsic current densities (about 5% larger than Jc_0). Figure 4 shows snapshots of the magnetization distribution for the case of the

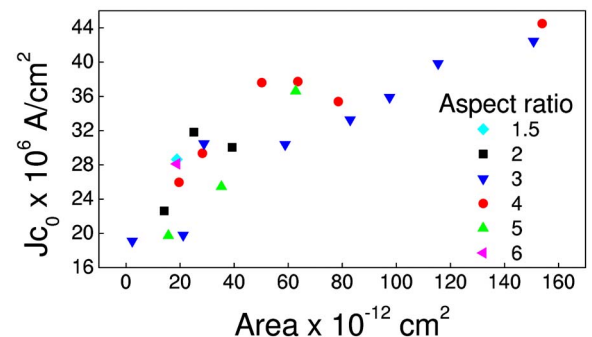


FIG. 3. (Color online) Micromagnetic simulation of the intrinsic switching current densities for devices with various sizes and aspect ratios.

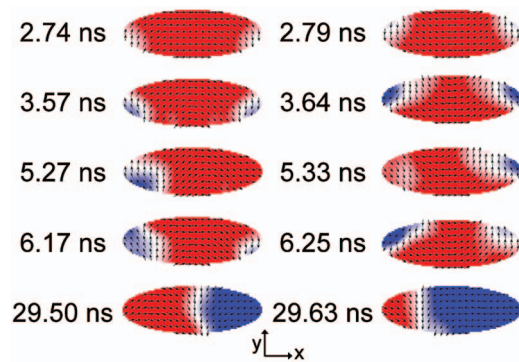


FIG. 4. (Color) Micromagnetic simulation snapshots of magnetization distribution of the $176 \times 60 \text{ nm}^2$ ellipse. The colors represent the average component of the magnetization along the x -axis (red positive, blue negative). $J = 34.7 \times 10^6 \text{ A cm}^2$. The time sequence is chosen so as to emphasize the oscillatory behavior. Each pair contains snapshots separated by a few tens of picoseconds.

$176 \times 60 \text{ nm}^2$ ellipse. For short times, the dynamics are described by excitation of end modes that oscillate 180° out of phase (antisymmetric) with gradually increasing amplitude. When the amplitude reaches a critical value ($M_x/M_y \approx 0.5$), the symmetry breaks down, followed by excitations that are not coherent and dynamics that are more chaotic in detail. We observe this behavior in all simulations of larger devices at currents close to the intrinsic switching current. To verify that the micromagnetic modeling produces results consistent with the single-domain results, we performed the same micromagnetic simulations with an exchange stiffness of $A = 2000 \times 10^{-12} \text{ J/m}$, 100 times larger than in the simulations discussed above (the single-domain model corresponds to infinite exchange stiffness). In this case, the switching proceeded via quasiuniform precessional dynamics, without the end-mode oscillations, and the results were the same as those obtained from Eq. (1), $J_{c0} = 20 \times 10^6 \text{ A cm}^2$ for the $104 \times 40 \text{ nm}^2$ and $177 \times 60 \text{ nm}^2$ ellipses. Simulations of small devices (e.g., $30 \times 10 \text{ nm}^2$) with $A = 20 \times 10^{-12} \text{ J/m}$ gave the same behavior.

The results presented here show that in larger devices the single-domain model predicts intrinsic current density values smaller than those experimentally observed. We believe that the reason lies in the occurrence of end-mode oscillations, which tend to dominate the reversal process when high-

speed current pulses are used. End-mode oscillations of odd symmetry correspond to the lowest-frequency normal mode for an ellipse.¹² Due to the dipole fields, end-mode oscillations with odd symmetry along the long axis are preferentially excited. The end-modes are initially excited because the spin torque is larger for the end spins, which at the onset of the current pulse are canted with respect to the injected spin polarization direction.

In conclusion, we have shown that J_{c0} , as experimentally measured with high-speed current pulses in elliptical spin valves, increases significantly with increasing device area, which is not predicted with a single-domain model. Micromagnetic simulations indicate a nonuniform and complex magnetization reversal process due to the excitation of end-mode oscillations in the larger structures. In these devices, the micromagnetic simulations better predict the values of the observed intrinsic switching current densities and their variation with device size. We show that micromagnetic effects can, in such circumstances, increase the intrinsic current densities above those predicted by the single domain reversal.

The authors thank M. Donahue (NIST-Gaithersburg) for assistance in applying OOMMF and M. Schneider (University of Montana-Missoula) for assisting in the experimental setup. This work was partially supported by the US Government.

¹J. A. Katine, F. J. Albert, R. A. Buhrman, E. B. Myers, and D. C. Ralph, *Phys. Rev. Lett.* **84**, 3149 (2000).

²J. C. Slonczewski, *J. Magn. Magn. Mater.* **159**, L1 (1996).

³J. Z. Sun, *IBM J. Res. Dev.* **50**, 81 (2006).

⁴Z. Diao, Z. Li, S. Wang, Y. Ding, A. Panchula, E. Chen, L.-C. Wang, and Y. Huai, *J. Phys.: Condens. Matter* **19**, 5209 (2007).

⁵G. Consolo, G. Finocchio, L. Torres, M. Carpentieri, L. Lopez-Diaz, and B. Azzarboni, *J. Magn. Magn. Mater.* **316**, 492 (2007).

⁶K. Ito, *IEEE Trans. Magn.* **41**, 2630 (2005).

⁷K.-J. Lee, A. Deac, O. Redon, J.-P. Nozieres, and B. Dieny, *Nat. Mater.* **3**, 877 (2004).

⁸S. Kaka, M. R. Pufall, W. H. Rippard, T. J. Silva, S. E. Russek, J. A. Katine, and M. Carey, *J. Magn. Magn. Mater.* **286**, 375 (2005).

⁹D. Lacour, J. A. Katine, N. Smith, M. J. Carey, and J. R. Childress, *Appl. Phys. Lett.* **85**, 4681 (2004).

¹⁰The Object Oriented MicroMagnetic Framework (OOMMF) project at ITL/NIST (<http://math.nist.gov/oommf/>).

¹¹J. Xiao, A. Zangwill, and M. D. Stiles, *Phys. Rev. B* **70**, 172405 (2004).

¹²R. D. McMichael and M. D. Stiles, *J. Appl. Phys.* **97**, 10J901 (2005).